

Electronic Supplementary Information (ESI) for

Synthesis and Internal Electric Field Dependent Photoreactivity of Bi₃O₄Cl Single-Crystalline Nanosheets with High {001} Facet Exposure Percentages

Jie Li,^{†‡} Lizhi Zhang,^{†*} Yujie Li,[‡] and Ying Yu[‡]

[†]Key Laboratory of Pesticide & Chemical Biology of Ministry of Education, Institute of Environmental Chemistry, College of Chemistry, Central China Normal University, Wuhan 430079, P. R. China.

[‡]Institute of Nanoscience and Nanotechnology, College of Physical Science and Technology, Central China Normal University, Wuhan 430079, P. R. China.

*Corresponding author. Phone/fax: +86-27-6786 7535.

Email address: zhanglz@mail.ccnu.edu.cn

Experimental Section

In a typical procedure, 4 mmol of Bi(NO₃)₃·5H₂O and 4 mmol of NaCl were added in 24 mL of distilled water at room temperature with continuous stirring, and then 36~38 wt % ammonia was added to this solution to adjust the pH value of solution to about 10.3. The resulting mixture solution (solution A) was stirred for 30 min and then poured into a 100 mL Teflon-lined stainless autoclave. The autoclave was allowed to be heated at 160°C for 18 h under autogenous pressure, and then air cooled to room

temperature. The resulting precipitates were collected, then washed with ethanol and deionized water thoroughly, and finally dried at 50 °C in air. We called the obtained sample BOC-91. For the preparation of BOC-95, 0.2 g of BOC-91 was swelled in isopropanol and gradually exfoliated under ultrasound radiation for 4 h. For the preparation of BOC-86, 0.2 g of BOC-91 were added into the solution A, followed by the hydrothermal treatment at 160°C for 18 h.

The powder X-ray diffraction (XRD) patterns of the samples were recorded on a Rigaku D/MAX-RB diffractometer with monochromatized Cu K α radiation ($\lambda = 0.15418$ nm). The morphology of the samples was observed with a JEOL 6700-F field-emission scanning electron microscope (SEM) and JEOL JSM-2010 high-resolution transmission electron microscopy (HRTEM). For TEM sample preparation, the powders were suspended in ethanol, and then a drop of this suspension was deposited onto a holey carbon film supported by a copper grid. The TEM specimen was dried in air prior to the TEM examination. UV-visible diffused reflectance spectra of the samples were obtained for the dry-pressed film samples with using a UV-visible spectrophotometer (UV-2550, Shimadzu, Japan). BaSO₄ was used as a reflectance standard in a UV-visible diffuse reflectance experiment. Photoluminescence (PL) spectra of the samples were recorded on a Fluoromax-Pluminescence spectrometer (Horiba Jobin Yvon Inc.). Electron spin resonance (ESR) spectra with 5, 5-dimethyl-1-pyrroline-N-oxide (DMPO) as the radical spin-trapped reagent were determined on a Bruker ESR 300E spectrometer. The concentration of DMPO was 0.2 mol/L, and the irradiation source was a 500 W Xe arc lamp with a 420 nm cutoff filter. Charge density of Bi₃O₄Cl nanosheets as function of pH was calculated by using K_1 and K_2 values obtained from the simultaneous potentiometric and conductimetric titrations.

The photocatalytic activity experiments on the degradation of salicylic acid (SA) were performed at ambient temperature using 500 W Xe arc lamp with a 420 nm cutoff filter as the light source. Typically, a 0.05 g amount of photocatalyst was added into 50 mL of 10 mg L⁻¹ SA aqueous solution in a container. Prior to irradiation, the suspensions were stirred in the dark for 1 h to ensure the adsorption/desorption equilibrium. During the degradation, the SA solution with photocatalyst was continuously stirred by a magnetic stirrer and the concentration of SA was monitored by colorimetry with a UV-visible spectrophotometer (UV-2550, Shimadzu, Japan).

The photoelectrodes were prepared according to a previously reported method. The indium doped tin oxide (ITO, China Southern Glass Co., Ltd., Shenzhen, China) substrates were cleaned by ultrasonication in distilled water, absolute ethanol, and isopropanol for 15 min sequentially. Both edges of the conducting glass substrates were covered with adhesive tape. Typically, the aqueous slurries of the Bi₃O₄Cl were spread on an ITO glass substrate with a glass rod, using adhesive tapes as spaces. The suspension was prepared by grinding 20 mg of Bi₃O₄Cl nanosheets, 40 µL of PEDOT-PSS (Sigma-Aldrich, 1.3-1.7%) aqueous solution and 200 µL of water, and the film was dried in air and annealed at 150 °C for 10 min. The photocurrents were measured by an electrochemical analyzer (CHI660D Instruments) in a standard three-electrode system with the samples as the working electrodes, a Pt foil as the counter electrode, and a saturated calomel electrode (SCE) as a reference electrode. A 500 W Xe arc lamp with a 420 nm cutoff filter was utilized as a light source. A 0.5 M Na₂SO₄ aqueous solution was used as the electrolyte.

Theoretical calculations were performed using density functional theory (DFT) as implemented in the VASP code. Three dimensional periodic boundary conditions were used to approximate an infinite solid.

Exchange-correlation effects were described through the generalized gradient approximation, within the Perdew-Burke-Ernzerhof (PBE) formalism. The core electrons (Bi:[Xe], Cl:[Ne], O:[He]) were treated within the projector augmented wave (PAW) method. The k-point density ($3 \times 3 \times 1$) and plane wave cutoff threshold (400 eV) were found to be well converged. The optical transition matrix elements were calculated within the transversal approximation and the PAW method. Structure and charge density visualization and analysis were performed using VENUS.

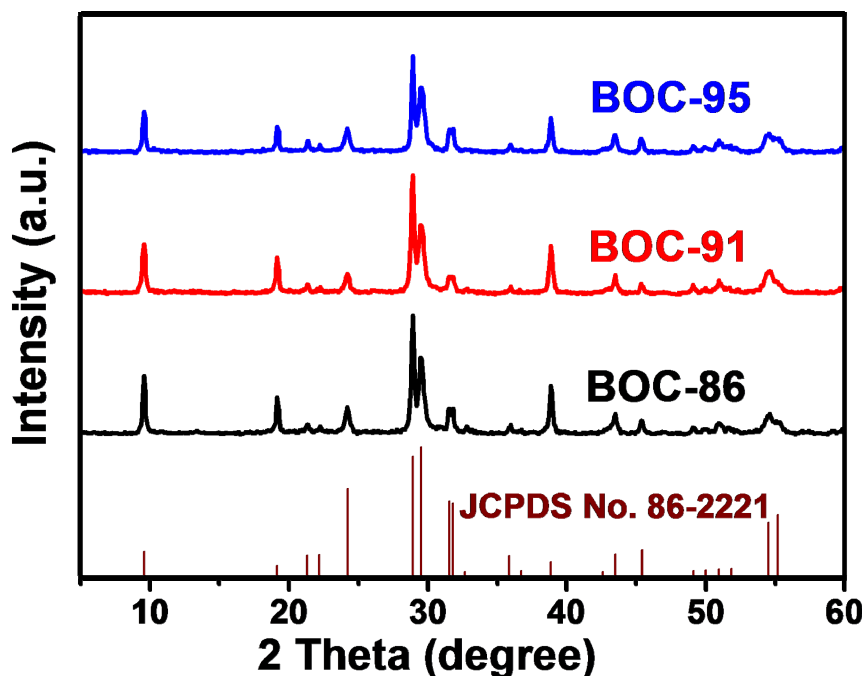


Fig. S1. XRD patterns of $\text{Bi}_3\text{O}_4\text{Cl}$ nanosheets with different $\{001\}$ facet exposure percentages.

XRD analysis revealed that with the $\{001\}$ facet exposure percentages increased, the XRD peak intensity of $\text{Bi}_3\text{O}_4\text{Cl}$ nanosheets gradually decreased, ruling out the contribution of high crystallinity on their photocatalytic activity.

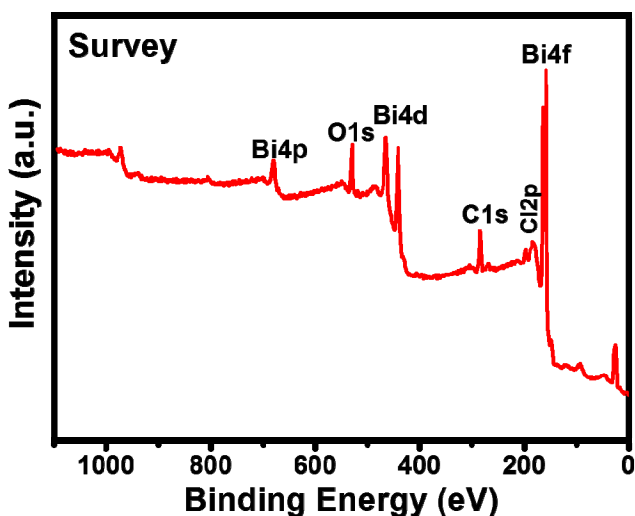


Fig. S2. XPS spectra of $\text{Bi}_3\text{O}_4\text{Cl}$ nanosheets.

The typical survey XPS spectrum of $\text{Bi}_3\text{O}_4\text{Cl}$ nanosheets indicated that the product consisted of Bi, O and Cl elements. Quantification calculated on the basis of the peaks areas of the Bi and Cl high resolution spectrum within experimental error gave the atomic ratio of Bi to Cl, which was 3.03:1.

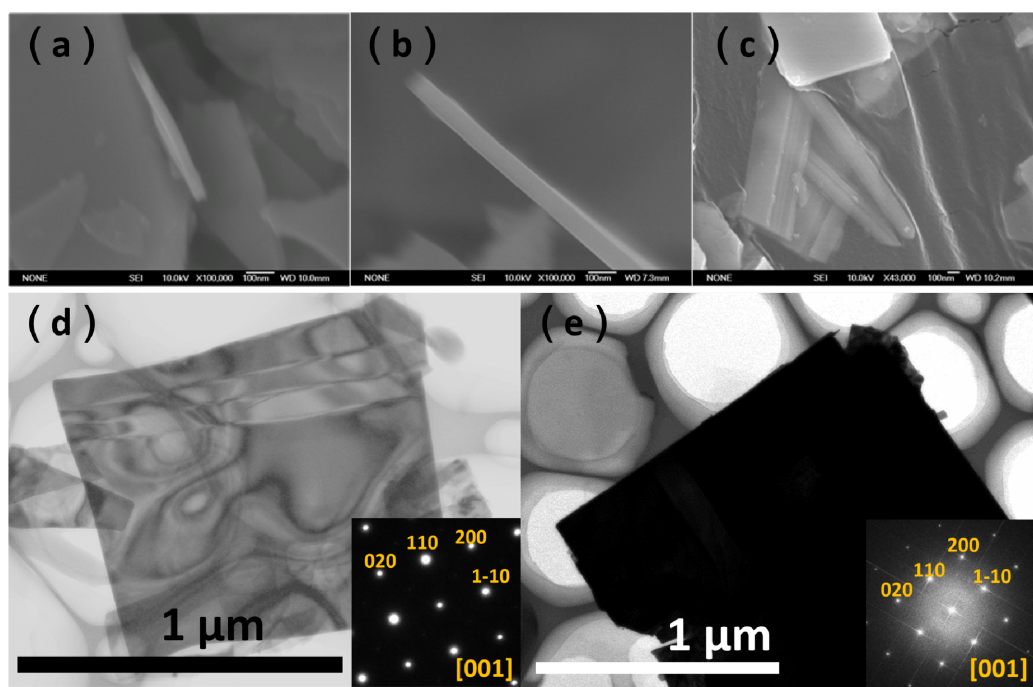


Fig. S3. SEM images of BOC-95 (a), BOC-91 (b) and BOC-86 (c). TEM images and SAED pattern of BOC-95 (d) and BOC-86 (e)

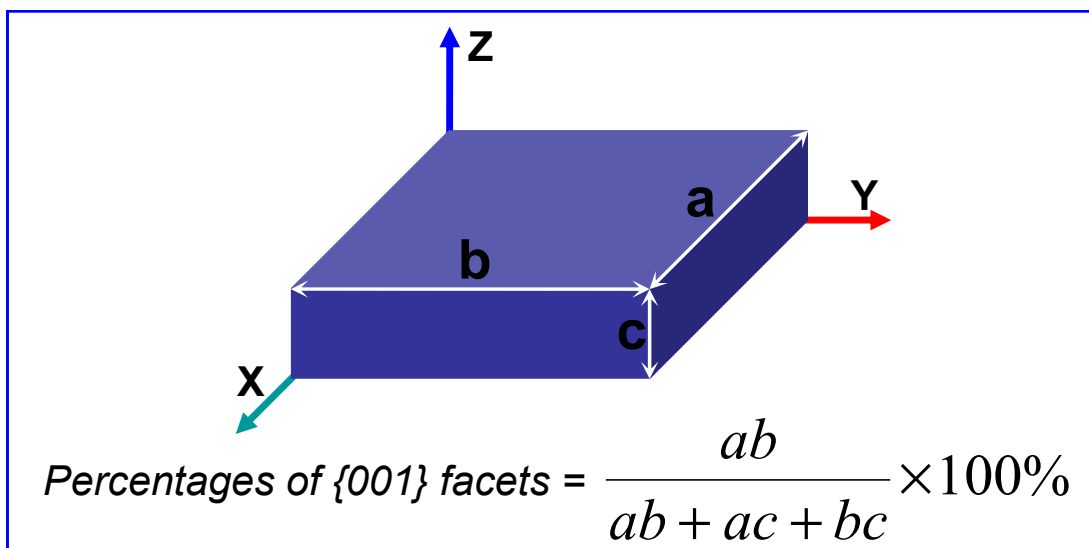


Fig. S4. Geometric diagram of $\text{Bi}_3\text{O}_4\text{Cl}$ nanosheets and the formula for calculating the $\{001\}$ facet percentages.

We employed liquid phase exfoliation and hydrothermal recrystallization to finely tune the exposed $\{001\}$ percentages of the as-prepared $\text{Bi}_3\text{O}_4\text{Cl}$ nanosheets (Figure 1e). It was reported that the layered materials could be exfoliated when the enthalpy of mixing was minimized in case that the surface energies of the nanosheets and the solvent matched each other with the aid of ultrasonication.¹ We thus swelled $\text{Bi}_3\text{O}_4\text{Cl}$ nanosheets in isopropanol and gradually exfoliated the nanosheets under ultrasound radiation with increasing the $\{001\}$ facet exposure percentage from 91% to 95% (Figure S3 and S4). While hydrothermal treatment of $\text{Bi}_3\text{O}_4\text{Cl}$ nanosheets in an aqueous solution of $\text{Bi}(\text{NO}_3)_3 \cdot 5\text{H}_2\text{O}$, NaCl and ammonia could decrease the $\{001\}$ facet exposure percentage from 91% to 86%.² We called the samples obtained with liquid phase exfoliation and hydrothermal recrystallization post-treatment BOC-95 and BOC-86 on the basis of their $\{001\}$ facet exposure percentage.

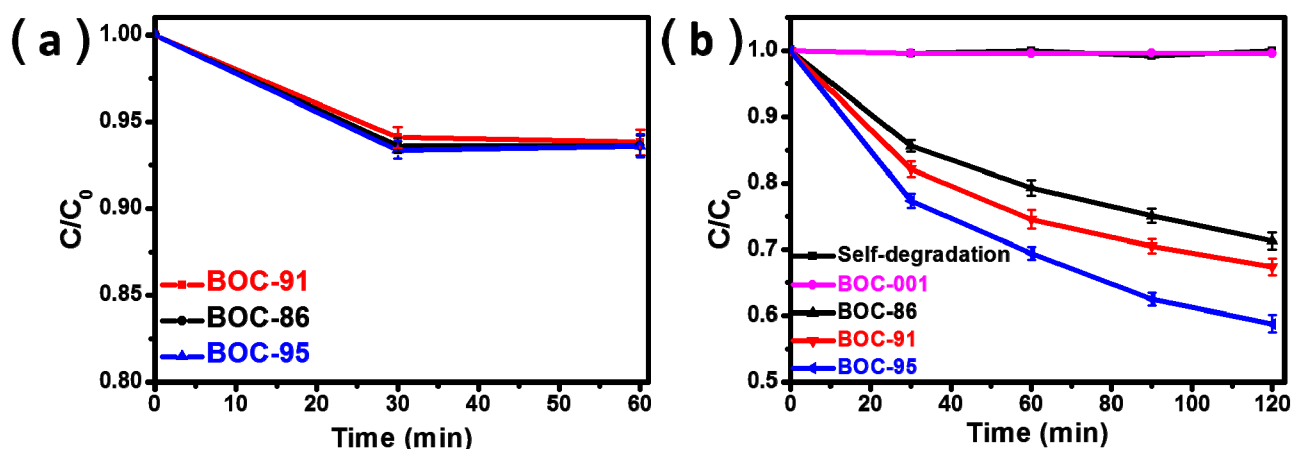


Fig. S5. (a) Time profiles of adsorption of SA in the dark. (b) Time profiles of photocatalytic degradation of SA under visible light irradiation ($\lambda > 420$ nm).

The photocatalytic properties of $\text{Bi}_3\text{O}_4\text{Cl}$ nanosheets with different $\{001\}$ facet exposure percentages were evaluated using SA as the probe molecule under visible ($\lambda > 420$ nm) light irradiation. For comparison, self-degradation of SA and its degradation over BOC-001 were also investigated. As shown in Figure S5b, SA was very stable under visible light in the absence of photocatalyst and the all $\text{Bi}_3\text{O}_4\text{Cl}$ nanosheets exhibited much higher photocatalytic activity than BiOCl nanosheets with exposed $\{001\}$ facets (BOC-001) under visible-light irradiation. SA could not be degraded over BOC-001 under visible light because BOC-001 with a wide-bandgap could not be excited by the incident visible light.

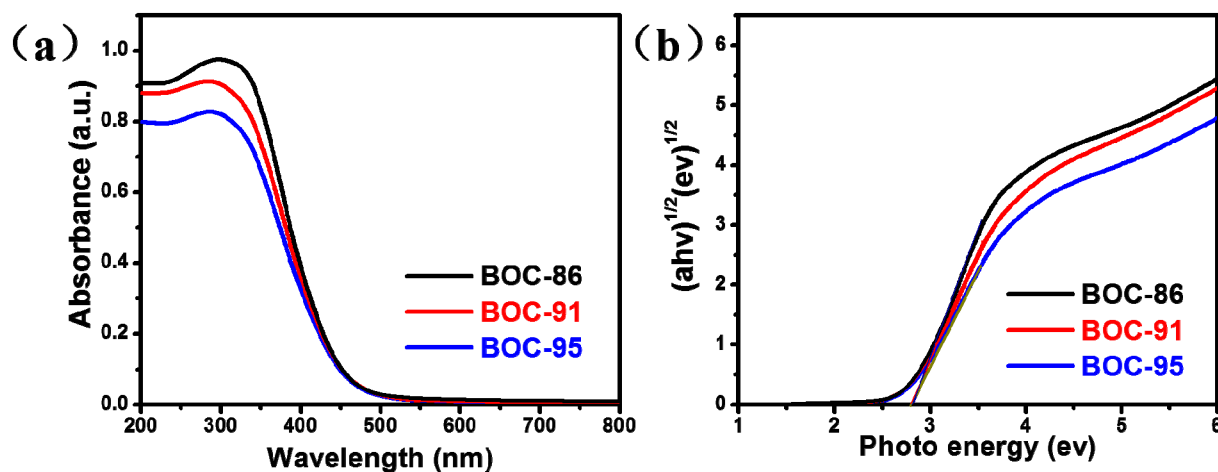


Fig. S6. a) UV-visible absorption spectra and b) plots of $(\alpha h\nu)^{1/2}$ versus energy ($h\nu$) for the band-gap energies of $\text{Bi}_3\text{O}_4\text{Cl}$ nanosheets with different $\{001\}$ facet exposure percentages.

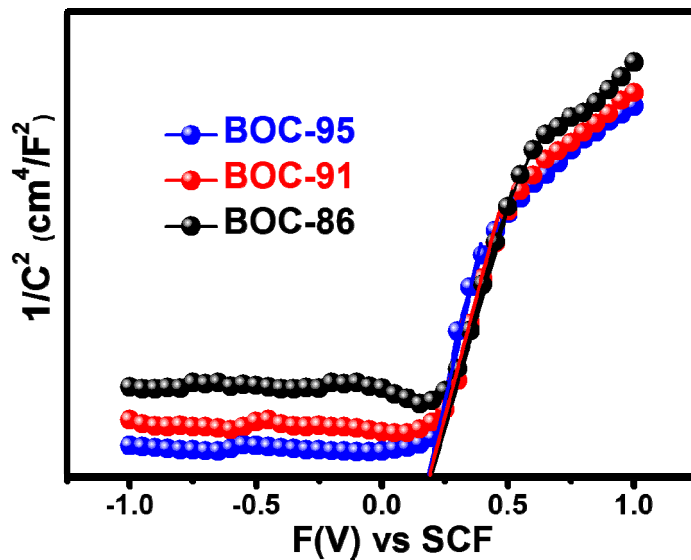


Fig. S7. Mott-Schottky plots of $\text{Bi}_3\text{O}_4\text{Cl}$ nanosheets with different percentages of exposed $\{001\}$ facets.

As the light harvesting and photoexcitation of a semiconductor depends on electronic structures, we utilized UV-Vis diffuse reflectance spectroscopy to investigate the electronic structures of $\text{Bi}_3\text{O}_4\text{Cl}$ nanosheets with different $\{001\}$ facet exposure percentages and found that the three samples possessed virtually the same photoabsorption edge (Figure S6a), suggesting the independence of their different

photocatalytic performance on the light harvesting and photoexcitation. The band gaps of the three samples obtained from plots of $(\alpha h\nu)^{1/2}$ versus photon energy ($h\nu$) (Figure S6b) were estimated to be 2.84 eV. Mott-Schottky plots (Figure S7) showed all the three samples had the same the flat band potential. Thus, the valence and conduction band potentials of the three nanosheets were almost identical, ruling out the influence of different photoredox ability of the three samples on their photoreactivity.

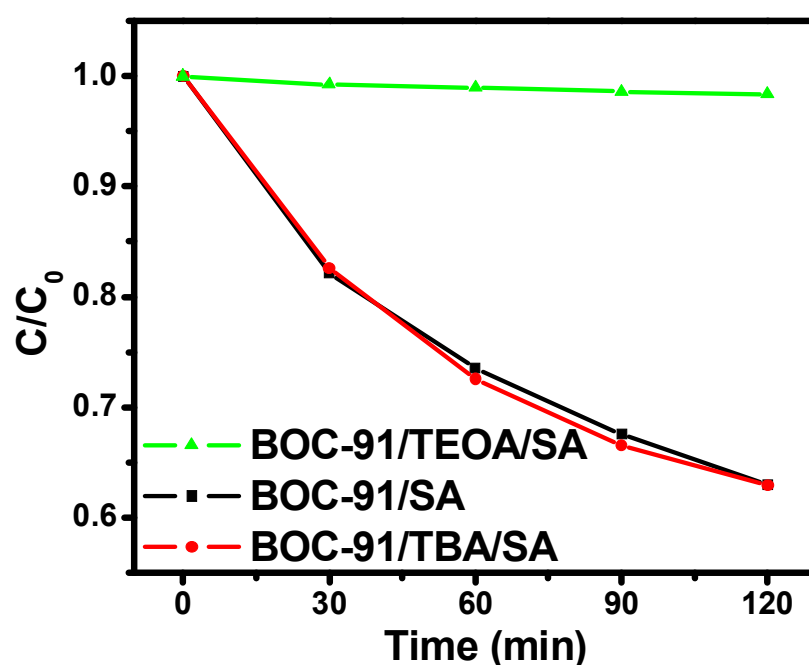


Fig. S8. Comparison of photocatalytic SA degradation over the BOC-91 in different photocatalysis systems under visible light irradiation ($\lambda > 420$ nm). TEOA and TBA were chosen as the hole and $\cdot\text{OH}$ scavengers, respectively.

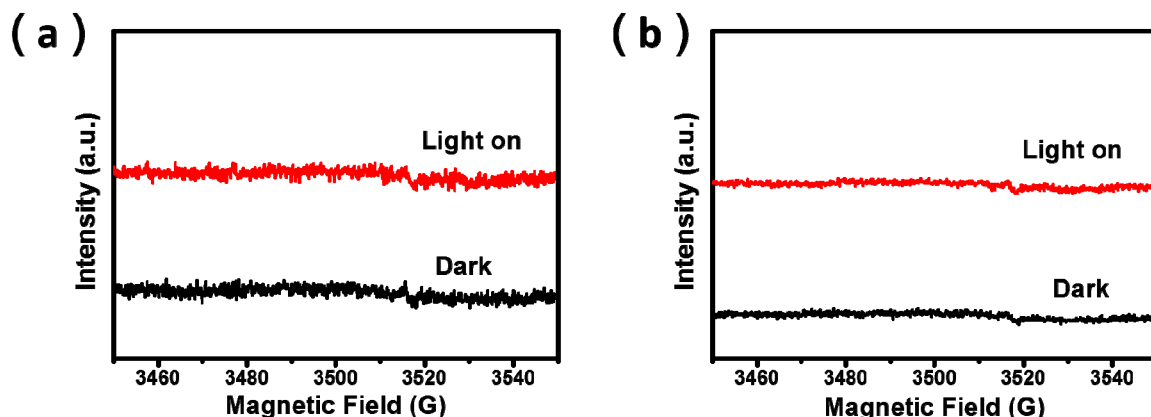


Fig. S9. (a) DMPO spin-trapping ESR spectra of $\text{Bi}_3\text{O}_4\text{Cl}$ nanosheets methanol dispersion for DMPO- $\cdot\text{O}_2^-$, (b) DMPO spin-trapping ESR spectra of $\text{Bi}_3\text{O}_4\text{Cl}$ nanosheets in aqueous dispersion for DMPO- $\cdot\text{OH}$.

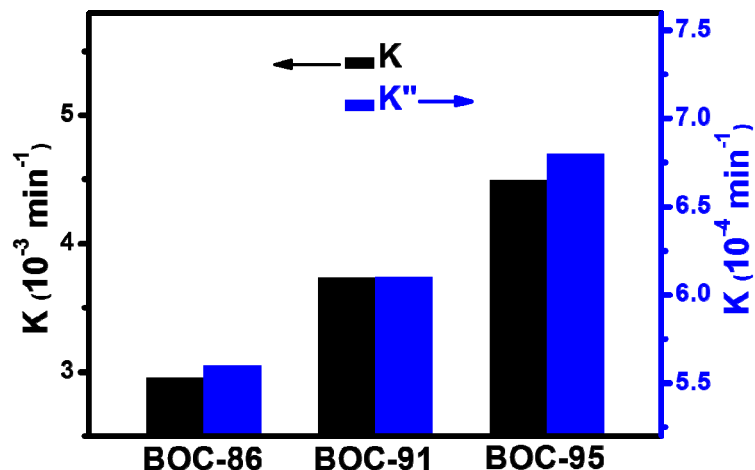


Fig. S10. Comparison of the apparent reaction rate constants before and after normalized simultaneously with both the surface area and the $\{001\}$ facet exposure percentages (K : the reaction rate constants; K'' : the reaction rate constants normalized with both the surface area and the $\{001\}$ facet exposure percentages).

Active species trapping experiments revealed that direct hole-dominant photooxidation was principally

responsible for the photodegradation of SA over the Bi₃O₄Cl nanosheets (Figure S8). No characteristic peaks of ·OH and ·O²⁻ in DMPO spin-trapping ESR spectra (Figure S9) further confirmed the hole-dominant photooxidation mechanism, which is ascribed to the lower standard redox potential of Bi⁵⁺/Bi³⁺ (E₀ = 1.59 V, at pH = 0) than that (1.99 V, at pH = 0) of ·HO/OH⁻.³ It is known that direct contact between the pollutant molecules and the surface of semiconductor is a prerequisite for hole-dominant photooxidation on the surface of the semiconductor.⁴ While surface property of semiconductor is crucial for their photoreactivity because a high density of surface unsaturated-coordinated atoms would cause a high surface energy for the crystal facet and a crystal with a higher percentages of reactive facet is usually more reactive in heterogeneous reactions. Therefore, we normalized photocatalytic degradation rate constants of BOC-86, BOC-91 and BOC-95 simultaneously with their percentages of {001} facets and surface areas to check if the surface property of Bi₃O₄Cl nanosheets is the major factor to determine their photoreactivity, and surprisingly found that the normalized rate constant still increased monotonously with increasing the percentages of {001} facets (Table S1). This result suggests that the photoreactivity of Bi₃O₄Cl nanosheets with high {001} facet exposure percentage is not dominated by their surface properties of {001} facets in this study.

Table S1. Structural information and photoactivity evaluation of $\text{Bi}_3\text{O}_4\text{Cl}$ nanosheets with different $\{001\}$ facet exposure percentages.

Sample	Average thickness (nm)	Average length (μm)	$P_{001}^{[a]}$ (%)	$S_{\text{BET}}^{[b]}$ ($\text{m}^2 \text{g}^{-1}$)	$K^{[c]}$ ($\text{min}^{-1} \times 10^{-3}$)	$K'^{[d]}$ ($\text{min}^{-1}, \times 10^{-3}$)	$K''^{[e]}$ ($\text{min}^{-1}, \times 10^{-3}$)
BOC-95	30	1.1	95	6.96	4.49	0.65	0.68
BOC-91	60	1.2	91	6.61	3.73	0.56	0.61
BOC-86	120	1.5	86	6.13	2.95	0.48	0.56

[a] Percentages of $\{001\}$ facets. [b] The specific surface area. [c] The reaction rate constants. [d] The reaction rate constants normalized with specific surface area. [e] The reaction rate constants normalized with both surface area and percentages of $\{001\}$ facets. ($K' = K/S_{\text{BET}}$; $K'' = K'/P_{001}$)

The mean values of thicknesses and lengths of more than 100 nanosheets were used as the average thickness and length of the nanosheets in Table S1.

Table S2. The pH dependence of open-circuit potentials with respect to the normal hydrogen electrode (NHE) for $\text{Bi}_3\text{O}_4\text{Cl}$ nanosheets with different $\{001\}$ facet exposure percentages.

Sample	Open-circuit potentials (V)			
BOC-95	0.060 (pH=5)	0.049 (pH=6)	0.043 (pH=7)	0.034 (pH=8)
BOC-91	0.056 (pH=5)	0.044 (pH=6)	0.038 (pH=7)	0.031 (pH=8)
BOC-86	0.052 (pH=5)	0.041 (pH=6)	0.036 (pH=7)	0.027 (pH=8)

Table 3. Surface charge density as a function of pH for Bi₃O₄Cl nanosheets with different {001} facet exposure percentages.

Sample	Surface charge density (C/m ²)			
BOC-95	0.39 (pH=5)	0.30 (pH=6)	0.25 (pH=7)	0.15 (pH=8)
BOC-91	0.31 (pH=5)	0.28 (pH=6)	0.24 (pH=7)	0.14 (pH=8)
BOC-86	0.28 (pH=5)	0.23 (pH=6)	0.19 (pH=7)	0.12 (pH=8)

Surface charge density of Bi₃O₄Cl nanosheets as function of pH was calculated by applying Eq. (1) and using K_1 and K_2 values obtained from the simultaneous potentiometric and conductimetric titrations. The equilibrium constants K_1 and K_2 can be experimentally determined by the application of Henderson–Hasselbach equation in the simultaneous potentiometric and conductimetric titration data. From equilibrium constants, the surface charge density of Bi₃O₄Cl nanosheets as function of pH values can be calculated by the following Eq. (1).

$$\rho_0 = \left(\frac{F}{A} \right) \left[\left(\frac{10^{-2pH} - K_1 K_2}{10^{-2pH} + 10^{-2pH} K_1 + K_1 K_2} \right) N_T \right] \quad \text{Eq. (1)}$$

Where F is the Faraday constant, A is the total surface area, NT is the total number of moles of surface sites, and K_1 and K_2 are the acid equilibrium constants.

REFERENCE

- (1) (a) J. N. Coleman, M. Lotya, A. O' Neill, S. D. Bergin, P. J. King, U. Khan, K. Young, A. Gaucher, S. De, R. J. Smith, I. V. Shvets, S. K. Arora, G. Stanton, H. Y. Kim, K. Lee, G. T. Kim, G. S. Duesberg, T. Hallam, J. J. Boland, J. J. Wang, J. F. Donegan, J. C. Grunlan, G. Moriarty, A. Shmeliov, R. J. Nicholls, J.

- M. Perkins, E. M. Grieveson, K. Theuwissen, D. W. McComb, P. D. Nellist and V. Nicolosi, *Science.*, 2011, **331**, 568; (b) S. B. Yang, Y. J. Gong, J. S. Zhang, L. Zhan, L. L. Ma, Z. Y. Fang, R. Vajtai, X. C. Wang and P. M. Ajayan, *Adv. Mater.*, 2013, **25**, 2452; (c) X. D. Zhang, X. Xie, H. Wang, J. J. Zhang, B. C. Pan and Y. Xie, *J. Am. Chem. Soc.*, 2013, **135**, 18; (d) Y. F. Sun, H. Cheng, S. Gao, Z. H. Sun, Q. H. Liu, Q. Liu, F. C. Lei, T. Yao, J. F. He, S. Q. Wei and Y. Xie, *Angew. Chem. Int. Ed.*, 2012, **51**, 8727.
- (2) (a) D. A. Payne, and S. Theokritoff, *Mater. Res. Bull.*, 1975, **10**, 437. (b) M. N. An'amt, S. Radiman, N. M. Huang, M. A. Yarmo, N. P. Ariyanto, H. N. Lim and M. R. Muhamad, *Ceram. Int.*, 2010, **36**, 2215. (c) V. I. Popolitov, B. N. Litvin and A. N. Lobachev, *Phys. Status. Solidi. A*, 1970, **3**, K1. (d) D. A. Payne, and J. L. Mukherjee, *Appl. Phys. Lett.*, 1976, **29**, 748.
- (3) (a) H. B. Fu, C. S. Pan, W. Q. Yao and Y. F. Zhu, *J. Phys. Chem. B*, 2005, **109**, 22432; (b) X. Xiao, C. Liu, R. P. Hu, X. X. Zuo, J. M. Nan, L. S. Li and L. S. Wang, *J. Mater. Chem.*, 2012, **22**, 22840; (c) M. Ge, L. Liu, W. Chen and Z. Zhou, *CrystEngComm.*, 2012, **14**, 1038.
- (4) (a) G. H. Dong, K. Zhao and L. Z. Zhang, *Chem. Commun.*, 2012, **48**, 6178; (b) G. H. Dong and L. Z. Zhang, *J. Mater. Chem.*, 2012, **22**, 1160.